

# Incommensurate–Commensurate Transition in the Geometric Ferroelectric LaTaO<sub>4</sub>

Grant W. Howieson, Shitao Wu, Alexandra S. Gibbs, Wuzong Zhou, James F. Scott, and Finlay D. Morrison\*

In memory of our co-author, colleague and friend, Prof. James (Jim) F. Scott, FRS who passed away on 6th April 2020 during the final stages of this study.

The layered perovskite LaTaO<sub>4</sub> has been synthesized to be stable in both (polar) orthorhombic and (nonpolar) monoclinic polymorphs at ambient conditions. Although the structural transition between monoclinic and orthorhombic phases has been well established, there is some controversy regarding a further, unidentified transition around 500 K. Here this is identified as an incommensurate–commensurate first-order transition between incommensurate  $Cmc2_1(\alpha 00)0s0$  and commensurate  $Cmc2_1$  orthorhombic phases. Transmission electron microscopy indicates partially ordered stacking of different structural units in *a*, identifying the local cause for the modulation, whereas variable temperature powder neutron diffraction has shown the overall macroscopic modulation vector,  $q \approx (0.456, 0, 0)$ —roughly a  $2.2 \times$  expansion in *a*, corresponding to an approximate  $11a$  commensurate superunit cell dimension. The modulation shows a continuous temperature dependence until transitioning to the basic (commensurate) cell at  $T_{IC-C}$ . Doping the interlayer La sites with smaller Nd cations stabilizes the incommensuration to higher temperature, suggesting the modulation is geometrically driven at the A site.

## 1. Introduction

Layered, perovskite-related ferroelectric phases, most commonly of the Ruddlesden-Popper, Aurivillius, and Dion-Jacobson types, have been widely studied. An additional family of layered compounds of general formula,  $A_nB_nX_{3n+2}$ , known as the [110]-phases due to the perovskite layering perpendicular to the {110} plane with respect to the cubic perovskite structure. The stoichiometry of these phases can also be expressed in terms of anion excess  $ABX_\gamma$ , where  $\gamma = 3+2/n$ ; the additional anions introduce cleavages of the octahedral corner sharing in the [110] plane, resulting in perovskite blocks *n* octahedra thick. The perovskite structure is realized at  $n = \infty$ , and so with decreasing *n*, the density of layering increases and the structure becomes increasingly anisotropic. In terms of ferroelectrics in this family,  $n = 4$  oxides such as Sr<sub>2</sub>Nb<sub>2</sub>O<sub>7</sub> and La<sub>2</sub>Ti<sub>2</sub>O<sub>7</sub> have been

widely studied,<sup>[1,2]</sup> while the highly planar  $n = 2$  family, BaMF<sub>4</sub> ( $M^{2+} = \text{Mg, Mn, Co, Ni and Zn}$ ),<sup>[3,4]</sup> has been studied both experimentally and theoretically for forty years now. Many of the latter fluoride phases are extremely interesting because of their multiferroic properties, strongly planar anisotropy (mechanical, electrical, and magnetic), and very high ferroelectric Curie temperatures, often above their melting points near 1000 K. However, as fluorides they have received almost no device interest.

Recently the more commercially interesting isomorphous  $n = 2$  oxide LaTaO<sub>4</sub> has been examined. However, its structures and the phase transitions between them have remained controversial, in particular that associated with the higher temperature dielectric anomaly  $\approx 500$  K.<sup>[5,6]</sup> Such ferroelectric [110]-phases are of particular current interest as they are examples of geometric or topological proper ferroelectrics whereby the polarization arises due to distortion driven purely by cation radii or geometric effects, rather than electronic effects such as the second-order Jahn–Teller effect (or pseudo second-order Jahn–Teller effect). In addition, these materials also often exhibit structural modulations known as incommensurations. When crystals develop an ionic modulation that has wavelength that is not a rational fraction of the original lattice constants they are called “incommensurate” (IC). Recently these modulations have been treated as an

G. W. Howieson, S. Wu, Prof. W. Z. Zhou, Prof. J. F. Scott,<sup>[†]</sup>

Dr. F. D. Morrison

EaStCHEM

School of Chemistry

University of St Andrews

St Andrews KY16 9ST, UK

E-mail: finlay.morrison@st-andrews.ac.uk

Dr. A. S. Gibbs

ISIS Facility

Rutherford Appleton Laboratory

Chilton, Oxon OX11 0QX, UK

Prof. J. F. Scott


SUPA

School of Physics and Astronomy

University of St Andrews

St Andrews KY16 9SS, UK

<sup>[†]</sup>Deceased April 6, 2020.

 The ORCID identification number(s) for the author(s) of this article can be found under <https://doi.org/10.1002/adfm.202004667>.

© 2020 The Authors. Published by Wiley-VCH GmbH. This is an open access article under the terms of the Creative Commons Attribution License, which permits use, distribution and reproduction in any medium, provided the original work is properly cited.

DOI: 10.1002/adfm.202004667

extra dimension, and have resulted in there being 775 (3+1)D space groups (rather than the 230 for three dimensions).<sup>[7]</sup> In this work, we reconcile the various hypotheses and show that LaTaO<sub>4</sub> exhibits an incommensurate transition, very similar to that in BaMnF<sub>4</sub>, but with a structure more closely related to Sr<sub>2</sub>Nb<sub>2</sub>O<sub>7</sub>.

BaMnF<sub>4</sub> ( $n = 2$ ) adopts the  $A2_1am$  space group and undergoes a nearly continuous displacive (as evidenced by underdamped soft optical phonons) phase transition near  $T = 250$  K to an incommensurate structure whose details depend upon sample preparation. Guggenheim and co-workers<sup>[8]</sup> showed it to involve a soft optical phonon branch at  $(0.392, 1/2, 1/2)$  and, rather uniquely among incommensurate phases, this modulation vector was found to be temperature independent. Later Scott and Blinc<sup>[9]</sup> suggested that this is the first step in a Devil's staircase at  $5a^*/13$ , and subsequent neutron studies<sup>[10]</sup> confirmed that there were indeed a series of such staircase jumps, which satisfy a formula that gives  $5a^*$  at  $T_{\text{lock-in}}$  and  $5a^*/13$  at the higher transition  $T_{\text{IC}}$ . The presence of such a Devil's staircase was independently confirmed by several different kinds of experiment by Hidaka et al. including X-ray diffraction,<sup>[11]</sup> specific heat,<sup>[12]</sup> and piezoelectric resonance.<sup>[13]</sup>

Previous investigations of LaTaO<sub>4</sub> have confirmed that this material forms an isostructural orthorhombic phase identical to the ferroelectric fluorides and first principles studies have calculated the polarization of the orthorhombic phase to be relatively large ( $36 \mu\text{C cm}^{-2}$ ).<sup>[14]</sup> The results of experimental studies have shown that despite forming in the polar  $Cmc2_1$  space group (the same as  $A2_1am$  reported for BaMF<sub>4</sub> compounds but with the  $a$  and  $c$  axes interchanged,  $b$  remains as the long axis), LaTaO<sub>4</sub> samples did not switch under high applied electric fields ( $<100 \text{ kV cm}^{-1}$ ),<sup>[5]</sup> a characteristic also present in some fluorides such as BaMnF<sub>4</sub> and BaFeF<sub>4</sub>.<sup>[3]</sup>

In fact, LaTaO<sub>4</sub> can be stabilized in one of two polymorphs at room temperature: a nonpolar monoclinic  $P2_1/c$  phase ( $m$ -LaTaO<sub>4</sub>) and the polar orthorhombic  $Cmc2_1$  ( $o$ -LaTaO<sub>4</sub>) phase discussed above. These polymorphs are shown in relation to the parent aristotype structure in Figure 1a. The room-temperature polymorph can be directed by the choice of annealing conditions or pressure,<sup>[15]</sup> or by doping with small amounts of Nd<sup>3+</sup> cations.<sup>[5]</sup> Such conditions favor the higher density monoclinic phase (theoretical density  $\rho_m = 7.816 \text{ g cm}^{-3}$  at 293 K), compared to the orthorhombic phase ( $\rho_o = 7.794 \text{ g cm}^{-3}$ ). The  $m$ -LaTaO<sub>4</sub> samples would transition into the  $Cmc2_1$  structure at  $\approx 440$  K on heating and transition back at  $\approx 300$  K on cooling (further details of this phase transformation will be reported in a subsequent manuscript). The orthorhombic phase remains present up until an unidentified phase transition around 500 K (and up to 670 K depending on Nd-doping content).

In this study, we identify the previously unknown phase transition at  $\approx 500$  K in the orthorhombic phase as being an incommensurate/commensurate (IC/C) transition. It is surprising to find that the structure is not modulated in the same way as found in isostructural BaMnF<sub>4</sub> where the modulation occurs along the polar axis ( $a$  in space group setting  $A2_1am$ ), but instead shares a similar incommensurate modulation of 0.4558 (at 483 K) in  $a$  (space group  $Cmc2_1$ ) to that found in the  $n = 4$  ferroelectric oxide, Sr<sub>2</sub>Nb<sub>2</sub>O<sub>7</sub>. Using a variety of complimentary techniques including electron microscopy and neutron

diffraction, we demonstrate that in LaTaO<sub>4</sub> the incommensuration arises from partial ordering of competing structural units in contrast with "continuous" modulation mechanisms reported for the isostructural  $n = 2$  BaMnF<sub>4</sub> and  $n = 4$  Sr<sub>2</sub>Nb<sub>2</sub>O<sub>7</sub> layered ferroelectric phases whose IC structures have been studied extensively.

## 2. Results and Discussion

### 2.1. Initial Structural Characterization

Materials were initially characterized in-house by powder X-ray diffraction (PXRD), making determination of  $o$ -/ $m$ -phase mixtures difficult and these were only later revealed through neutron diffraction. Multiphase Rietveld refinement of powder neutron diffraction (PND) data, Figure 1b,c, shows that  $o$ -LaTaO<sub>4</sub> samples typically contained  $\approx 10$  wt%  $m$ -LaTaO<sub>4</sub> impurity while  $m$ -LaTaO<sub>4</sub> samples were relatively single phase ( $<1$  wt%  $o$ -LaTaO<sub>4</sub>).

Although refinements show good general agreement of the  $Cmc2_1$  model and the neutron data for the orthorhombic polymorph at 323 K (but with 10 wt% monoclinic phase), closer inspection of the 2.25–2.60 Å range reveals three peaks which are not accounted for by possible LaTaO<sub>4</sub> structures or any possible tertiary phase (inset of Figure 1c). The presence of these peaks in PND data were temperature dependent and their emergence at  $\approx 500$  K on cooling (and disappearance on heating) coincides with the dielectric anomalies observed in this study, Figure 1d,e, and previously.<sup>[5,6]</sup> This suggests that these peaks are satellites of main reflections and hence allude to some form of commensurate (resulting in a supercell) or incommensurate modulation.

Dielectric data clearly indicate the presence of successive phase transitions as a function of temperature for each polymorph of LaTaO<sub>4</sub>, Figure 1d,e, and the data are in good agreement with previous studies.<sup>[5,6]</sup> A large thermal hysteresis is present in the data from the " $m$ -LaTaO<sub>4</sub>" sample (Figure 1d), indicating a first-order phase transition between the monoclinic  $P2_1/c$  and the orthorhombic  $Cmc2_1$  phase at  $T_{m-o} \approx 440$  K on heating and  $\approx 300$  K on cooling. A second peak with little thermal hysteresis is observed at  $\approx 500$  K. The orthorhombic samples (Figure 1e) obviously lack any peak associated with  $T_{m-o}$  and instead exhibit only the higher temperature peak at approximately the same temperature ( $\approx 500$  K). As shown below this feature is associated with an incommensurate to commensurate transition ( $T_{\text{IC-C}}$ ). The small discrepancy in  $T_{\text{IC-C}}$  between polymorphs is attributed to the conditions required to stabilize each structure, which produced quite different sample qualities.

It is interesting to note that this high temperature dielectric anomaly has been noted in previous studies and was speculated to be a ferroelectric–antiferroelectric (FE-AFE) transition<sup>[5]</sup> or a ferroelectric–paraelectric (FE-PE) transition,<sup>[6]</sup> but this was never fully explored. In this study, the broadness of this dielectric anomaly was initially thought to be indicative of a second-order phase transition caused by two cooperative distortion modes involving the tilt of TaO<sub>6</sub> octahedra, but this was dispelled by acquisition of neutron and Raman data which showed a clear first-order nature of the transition. Further examination of the nature of the transitions by Raman and resonant ultrasound spectroscopy will be communicated in a

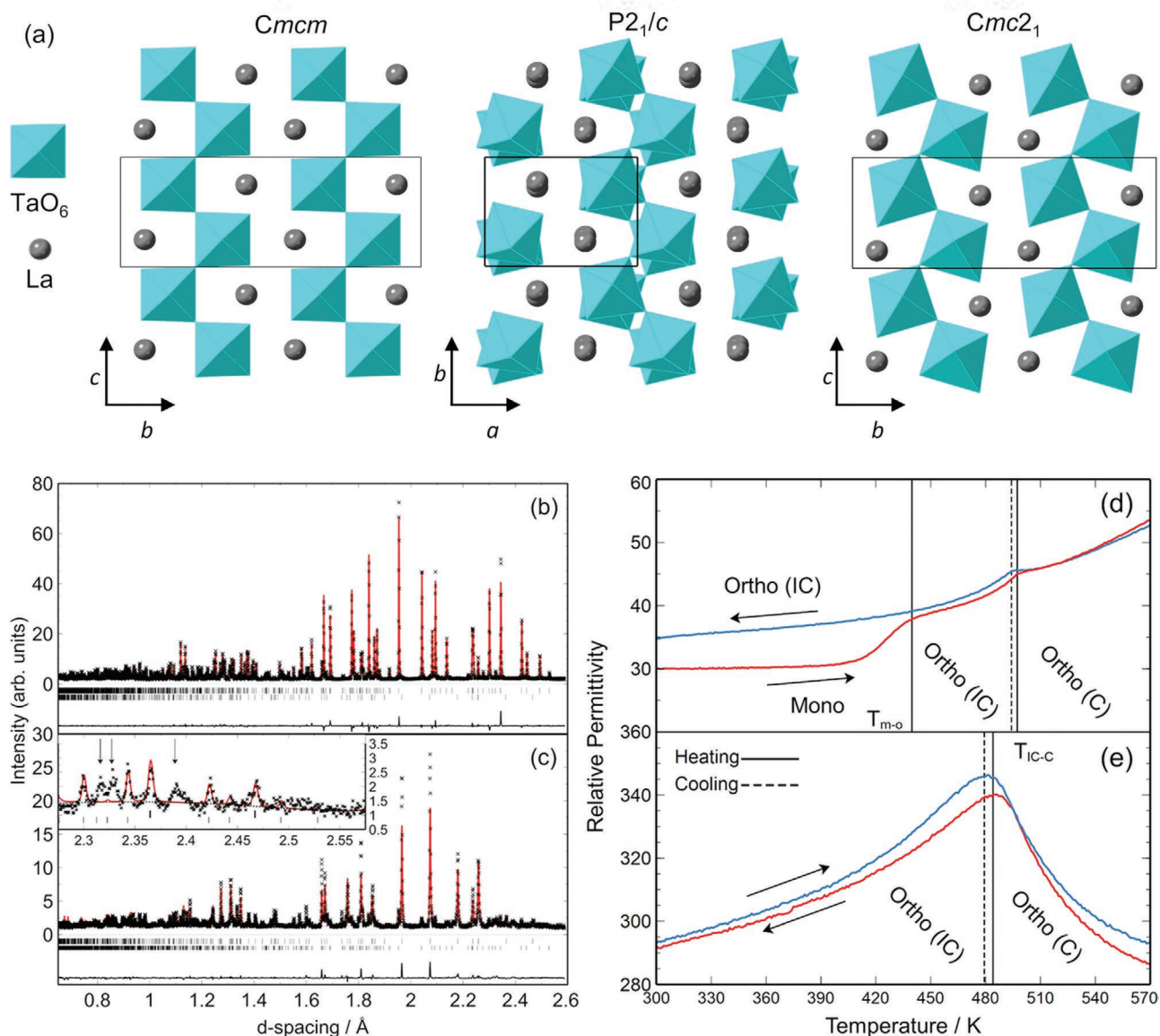


**Figure 1.** a) Parent, nonpolar  $Cmcm$   $ABX_4$  structure (left); nonpolar  $P2_1/c$  structure (middle) with antiphase tilting; polar  $Cmc2_1$  structure (right), where polarity arises from in-phase tilting of octahedra coupled with displacement of La cations. Two-phase Rietveld refinement profiles of PND data at 323 K in b) (commensurate) monoclinic  $P2_1/c$  and c) orthorhombic  $Cmc2_1$  space groups: the  $m$ - $LaTaO_4$  has <1 wt%  $o$ - $LaTaO_4$  with a  $\chi^2$  value of 6.647 for 46 variables ( $R_{wp} = 4.7\%$ );  $o$ - $LaTaO_4$  fit yields a  $\chi^2$  value of 5.804 for 68 variables with 10 wt%  $m$ - $LaTaO_4$  ( $R_{wp} = 9.1\%$ ). Inset of (c) indicates additional reflections associated with the incommensurate modulation. Dielectric spectroscopic data for samples initially in d) monoclinic and e) orthorhombic polymorphs at room temperature. d)  $m$ - $LaTaO_4$  shows two dielectric anomalies: one corresponding to the transition to the (IC) orthorhombic phase on heating at 440 K ( $T_{m-o}$ ) and one at 500 K corresponding to the IC-C transition ( $T_{IC-C}$ ) which occurs at  $\approx 500$  K on both heating and cooling. e)  $o$ - $LaTaO_4$  is synthesized in the IC orthorhombic phase and as such only presents  $T_{IC-C}$  on heating and cooling, occurring at  $\approx 490$  K.

subsequent paper, including the monoclinic–orthorhombic transition. An investigation of this transition by variable temperature PXRD (VT-PXRD) did show a clear change in lattice parameters but the limitations of X-ray diffraction prevented the exact nature of the structural change to be determined. Data at either side of this transition could be fitted reasonably well to the same  $Cmc2_1$  model, hence dismissing the assumption that this was a transition to the paraelectric  $Cmcm$  phase. It is also noted that investigations by Vullum, et al.,<sup>[15]</sup> and Cava and Roth<sup>[16]</sup> show  $LaTaO_4$  maintains the  $Cmc2_1$  space group up to at least 570 K.

The main reflections of the variable temperature PND data could be fitted over the entire temperature range using two  $Cmc2_1$  models with slightly different unit cell dimensions, **Figure 2a**. At temperatures close to  $T_{IC-C} \approx 500$  K, both “low-temperature” (LT) and “high-temperature” (HT)  $Cmc2_1$  phases coexist, consistent with a first-order transition.

Variable temperature PND data collected across the LT–HT phase transition are shown in **Figure 2c** as a contour plot, showing the change in main lattice peak positions and disappearance of superlattice peaks on heating. The first, most noticeable feature of this plot is the abrupt change in position

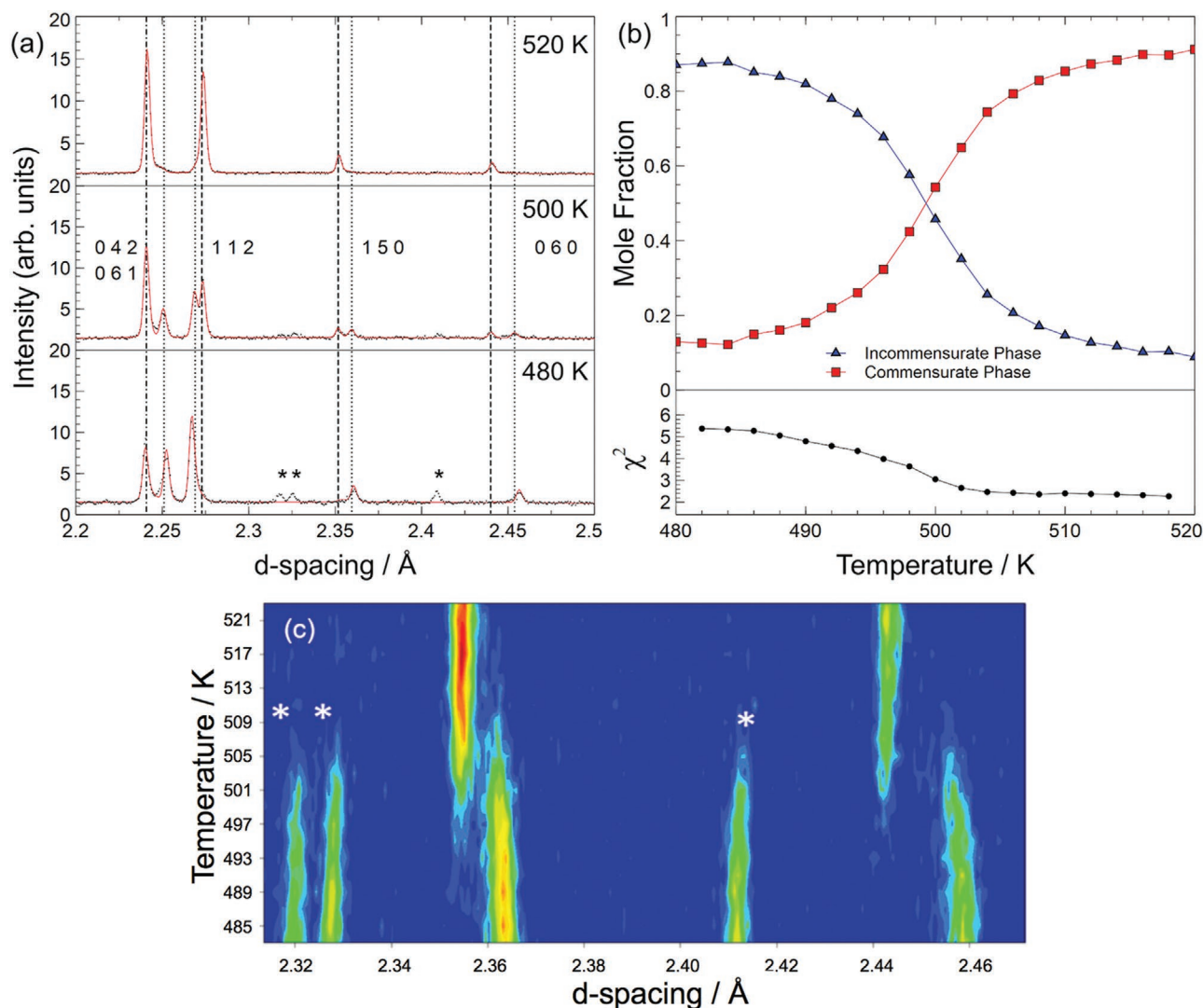


**Figure 2.** a) Section of Rietveld refinement profiles for *o*-LaTaO<sub>4</sub> at selected temperatures on cooling: data at 523 K (top) can be fitted by a “high-temperature” *Cmc*<sub>2</sub> model only; a two-phase refinement with both the “high-temperature” and “low-temperature” models, showing clear phase coexistence during the transition (middle); a low-temperature model can be used to fit data at 483 K (bottom). Dot-dash and dotted lines indicate reflections for high- and low-temperature models, respectively. Additional satellite peaks at 480 K associated with the incommensurate phase are indicated by asterisks. b) Phase fractions of LT (IC) and HT (C) *Cmc*<sub>2</sub> phases as a function of temperature show behavior consistent of a first order transition; the poorer goodness-of-fit at low temperature is due to the absence of fitting of satellite peaks is reflected in the larger  $\chi^2$  values. c) “Heat map” showing relative intensity of peaks in the PND data across the IC-C transition (483–523 K). In addition to a discontinuity in lattice parameters a region of phase coexistence can be clearly identified. The disappearance of the satellite reflections (\*) on heating is also evident.

of the main reflections of the LT and HT phases, again indicating a first-order transition. The satellite peaks at  $\approx 2.32$ – $2.33$  and  $2.41$  Å (indicated in the inset of Figure 1b) clearly disappear on heating into the HT phase, again consistent with some form of modulation in the LT phase.

Rietveld refinements of PND data were carried out using one or both of the two (LT and HT) *Cmc*<sub>2</sub> models each with slightly different lattice parameters. All reflections in the HT phase can be accounted for by the standard *Cmc*<sub>2</sub> model. The Rietveld refinements here do not take into account any modulation in the LT structure, and hence only the main reflections are fitted and the intensity associated with the superlattice peaks is ignored. This is reflected in the  $\chi^2$  value (goodness-of-fit), Figure 2b, which improves as the additional

reflections associated with the IC modulation disappear. The fractions of LT and HT phases determined by these refinements show a smooth variation across the transition with a region of coexistence consistent with a first-order transition.

Refinement of the main reflections of each of LT–HT phases allowed comparisons to be made between the average structures (Figure 3). The largest difference observed between the two structures is the large expansion in the *b* axis, implying that the octahedral “sheets” are not packing as closely together in the LT phase as a result of the modulation. The contraction of the *a* and *c* axes are much less significant than the *b* axis expansion (note the smaller axis ranges for *a* and *c* parameters) and hence the average unit cell volume of the LT (IC) phase is larger than the HT (C) phase.

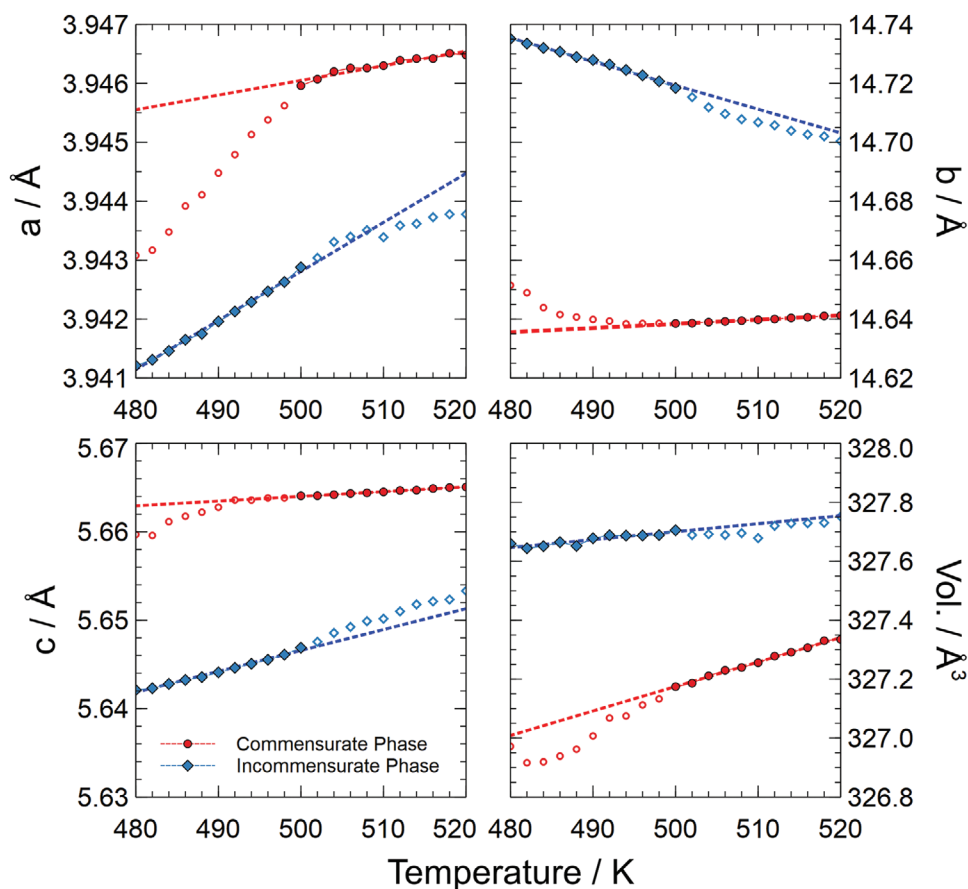


**Figure 3.** Lattice parameters of the low-temperature (IC) [blue diamonds] and high-temperature (C) [red circles] phases at the IC-C transition (483–523 K). Solid markers indicate data that were interpreted from regions where the phase is most prominent. Open markers represent regions where the phase fraction of the second phase is low, and subsequently associated values are less reliable. A linear relationship with temperature is assumed and lattice parameters are extrapolated from regions with greater confidence.

## 2.2. Identification of the Incommensuration–Electron Microscopy

Figure 4a shows a selected area electron diffraction (SAED) pattern of *o*-LaTaO<sub>4</sub> viewed down the [001] direction of the

(LT) orthorhombic unit cell with  $a = 3.9349 \text{ \AA}$ ,  $b = 14.7566 \text{ \AA}$ ,  $c = 5.6326 \text{ \AA}$ , space group  $Cmc2_1$ . The main diffraction spots can be indexed onto this basic unit cell with (100) and (010) spots absent. It is found that, along the [010] zone axis, no extra spots corresponding to any superstructures are seen. However, on

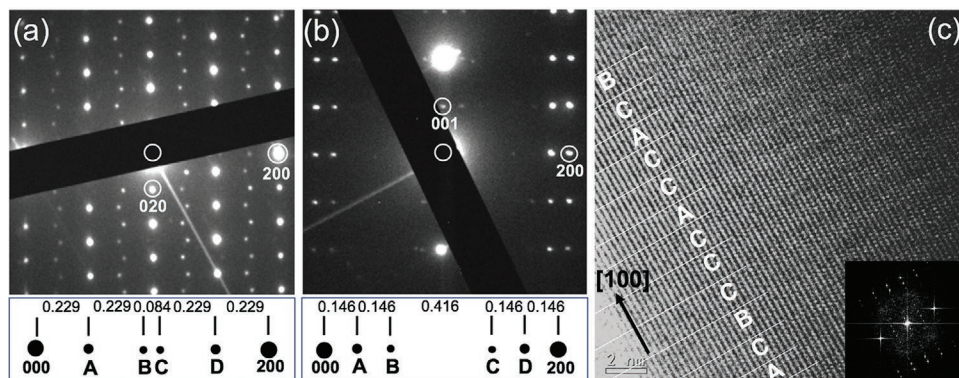


**Figure 4.** SAED patterns and HRTEM image of *o*-LaTaO<sub>4</sub>. a) SAED pattern of a particle view down the [001] zone axis. b) SAED pattern of another particle on the projection of the [010] direction. The positions of the satellite spots are marked below the two SAED patterns. c) HRTEM image with FFT (inset) corresponding to (b). The thicknesses of the blocks are marked, A: 11.7, B: 13.8, and C: 15.6 Å.

the [100] direction, some satellite spots are visible. These weak spots are not at positions of simple fractions, but in segment of the distance from (000) to (200) with separations of “0.229, 0.229, 0.084, 0.229, 0.229” as shown in Figure 4a. The value of 0.229 falls in between 0.20 (1/5) and 0.25 (1/4), and cannot be generated from a simple fraction. Therefore, these weak spots are diffraction peaks from an incommensurate superstructure.

To understand the formation mechanism of an incommensurate superstructure, it is possible to derive a commensurate superunit cell from it with reasonable dimensions. Such a hypothetical unit cell must contain two or more types of blocks (or two superstructural vectors), since single blocks can only form a commensurate superstructure. If these blocks are randomly arranged along a certain direction, diffused diffraction patterns arise. The situation is similar to disordered layered defects.<sup>[18]</sup> If the blocks are perfectly ordered, a commensurate superstructure forms. If they are partially ordered, the superstructure becomes incommensurate.<sup>[19,20]</sup> Accordingly, if the satellite spot “A” along the [100] direction in the SAED pattern of Figure 4a is shifted from 0.229 to 0.227, leading to a segmentation of “0.227, 0.227, 0.092, 0.227, 0.227” or simply “5, 5, 2, 5, 5,” the smallest approximate superstructure is 11-fold along this direction and the satellite spots can be indexed to A: (500)<sub>s</sub>, B: (10 00)<sub>s</sub>, C: (12 00)<sub>s</sub>, and D: (17 00)<sub>s</sub>, (where the subscript “s” indicates superstructure). The incommensurate structure can be attributed to partial ordering of two blocks, M and N, with dimensions of 6*m* and 5*m*, where *m* is a half of the basic unit cell parameter *a*. These blocks are relatively stable and can be connected to each other in different manners along the *a* axis, with very small difference in lattice energy, e.g., M–M, N–N, and M–N. When ordering from 2M and 2N blocks occurs, an 11-fold commensurate superstructure can be constructed. The appearance of the satellite spots may be attributed to a combination of diffraction peaks from M and N. As a general property of incommensurate structures, the ratios of the blocks, M: N and their permutations in different particles or in different areas of a particle would be variable. Consequently, the positions of the satellite spots in the SAED patterns would shift. Figure 4b shows an SAED pattern from another *o*-LaTaO<sub>4</sub> particle, viewed down the [010] axis. No superstructure is observed along the [001] direction, except that the originally absent (001) spot appears. Some weak satellite spots along the [100] direction are found again. However, their positions are different from those in Figure 4a, having fractions between (000) and (200) spots, “0.146, 0.146, 0.416, 0.146, 0.146.” The spot “A” is at a position between 1/7 (0.143) and 1/6 (0.167), but much close to the former. An approximate commensurate unit cell is sevenfold along the [100] axis. The spots in Figure 4b can be indexed onto A: (200)<sub>s</sub>, B: (400)<sub>s</sub>, C (10 00)<sub>s</sub>, and D: (12 00)<sub>s</sub>. The corresponding high-resolution transmission electron microscopy (HRTEM) image in Figure 4c indeed shows blocks along the [100] direction. Careful measurement reveals that there are three different thicknesses of the blocks, 11.7, 13.8, and 15.6 Å, which could be expressed as M (6*m*), O (7*m*) and P (8*m*), *m* = *a*/2. The appearance of the satellite diffraction spots can be attributed to a combination of diffraction peaks from these blocks. The hypothetical sevenfold superunit cell may contain 2O or M + P. In the real incommensurate structure, more blocks with partial ordering may exist. Therefore, when different areas are chosen to create fast Fourier transform

(FFT) patterns, a shift in the satellite spots is observed from one area to another. The proposed commensurate superstructure consisting of blocks, which contain elements of structural origin, is a simplified model to help understand the formation mechanism of the incommensurate superstructure.

### 2.3. Determination of Macroscopic Modulation

Jana2006 was used in determining the modulated structure from variable temperature PND data. Initial estimates of the modulation vector could be taken from electron microscopy and refined to account for all satellite peaks. The superspace group (SSG) was taken from a study of comparable *n* = 4 materials (e.g., Sr<sub>2</sub>Nb<sub>2</sub>O<sub>7</sub>) where there is a similar modulation observed in the *a* axis.<sup>[1,2]</sup> Although these *n* = 4 analogs have a modulation vector of *q* ≈ (0.5, 0, 0) and is similar to the doubling of the *a* axis in BaMnF<sub>4</sub> (*A*<sub>2</sub>am space group setting), reported by Hidaka;<sup>[21]</sup> it is important to note that due to the alternate space group setting the incommensuration in BaMnF<sub>4</sub> lies along the polar axis, but in the *n* = 4 oxides the incommensuration is orthogonal to the polarization. Given the similarities between the reported modulations in A<sub>2</sub>B<sub>2</sub>O<sub>7</sub> ferroelectrics and the candidate modulation vectors determined from TEM here, a modulation vector of approximately *q* = (0.5, 0, 0) was used as an initial value in refinements of data at 483 K. This resulted in a final value of *q* = (0.456, 0, 0) for LaTaO<sub>4</sub> at 483 K. Refining the PND data using the *Cmc*2<sub>1</sub>(*α*00)0*s*0 SSG, with a maximum satellite index of 3, gave a satisfactory fit of all reflections, with an overall  $\chi^2 = 2.57$  (*R*<sub>wp</sub> = 5.6%) across two HRPD detector banks (Figure 5).

The simplest modulation to consider is the displacement of the La<sup>3+</sup> cations, shifting into and away from the interstitial sites between the octahedral planes. A similar feature is observed in Sr<sub>2</sub>Nb<sub>2</sub>O<sub>7</sub>, where displacement of interstitial Sr cations is described as a means of resolving abnormally short bond lengths caused by unusual bonding environments—a product of the planar nature of the material.<sup>[1]</sup> This is assumed to be a mechanism also applicable to LaTaO<sub>4</sub>. The normal perovskite bonding environment is lost for the A cations in this type of structure: the interstitial A cation sites have tenfold coordination environment with an irregular geometry. The basic La–O bonds are shorter than the ideal bond length of the standard perovskite environment and the modulation is a mechanism to rectify this by varying the La positions with an accompanying tilt of the octahedra.

In both Sr<sub>2</sub>Nb<sub>2</sub>O<sub>7</sub><sup>[1]</sup> and La<sub>2</sub>Ti<sub>2</sub>O<sub>7</sub>,<sup>[2]</sup> the modulation is described by a simple sinusoidal atomic modulation function (AMF) which produces single maxima and minima in the displacement of Sr and La from the basic A site coordinates, representing the shift of each atom to a more favorable position. Although a similar treatment using the results of PND analysis is possible here, the electron microscopy data clearly indicates that the discontinuous stacking of similar orthorhombic cells creates the incommensurate structure. It is then evident that the partially ordered nature of the stacking of these cells in *a* would not allow the macroscopic structure of the IC phase to be determined by a simple AMF. The neutron diffraction analysis therefore gives the long-range average repeating unit of the IC

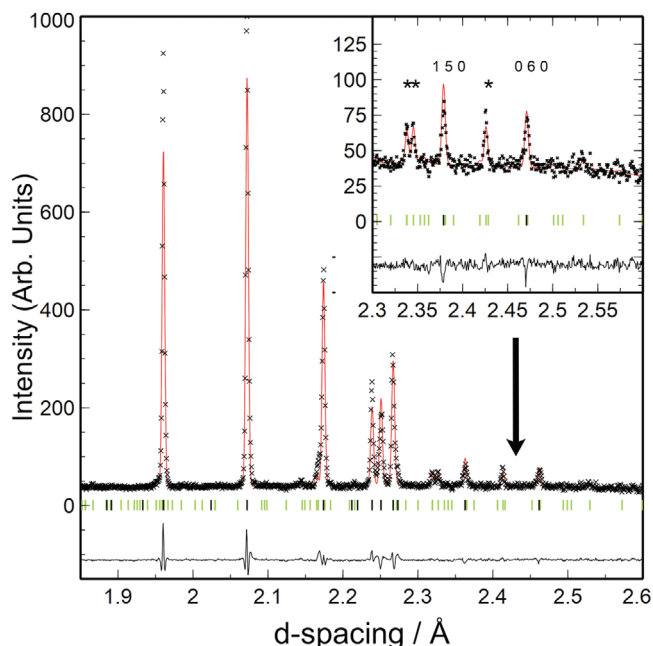


**Figure 5.** Rietveld refinement (using Jana2006) of PND data at 483 K for the highest resolution detector bank (HRPD bank1) with a final, refined, modulation vector  $q = (0.456, 0, 0)$  and with  $\chi^2 = 2.57$ . Main reflections are shown by black tick marks and satellite reflections (\*) are denoted by green tick marks.

phase of  $\text{LaTaO}_4$  and can be described by a modulation vector  $q \approx (0.456, 0, 0) \rightarrow \approx 2.2$  unit cells in  $a$ , i.e., close to a commensurate supercell of  $11a$ . The fact that this modulation vector assumes a value just above a commensurate 11 times expansion in  $a$  suggests that a combination of the M ( $6m$ ) and N ( $5m$ ) units with the former slightly more prominent is probably an appropriate construction.

## 2.4. Structural Units

Refinement of the PND data allowed a rough model of the atomic structure to be built, where a similar modulation to other layered perovskites is observed. The structure is composed of regions of varying degrees of cation displacement with an accompanying octahedral tilt and the model, whose repeating distance spanned approximately 11 unit cells in  $a$ , is able to be broken down into the blocks/supercells (Figure 6a) identified by HRTEM. These supercells are labeled M and N, and are as described previously, where they assume a thickness of  $6m$  and  $5m$ , respectively ( $m = a/2$ ). These structural units emerge as a product of the displacement of the La cations and resulting tilt of the surrounding octahedra, which acts as a means of improving overall bonding of La. However, the tilting of the octahedra would inevitably generate lattice strain in the octahedral layers. A natural way to release such a strain is that, over a certain distance, the octahedral tilting changes its manner. This argument deals with the principle of formation of block structures and a schematic drawing for this supercell formation is shown in Figure 6a. The nature of the tilting in each of these units predicts that certain rules are followed when these units order and this is illustrated in Figure 6b. M units stack along the  $a$  axis freely and are related by a translational symmetry. N units, however, dictate that neighboring units are also shifted by  $1/2$  unit cell in  $b$ —though the tilt system also forbids any stacking of different unit cells in  $b$  and so prohibits any supercells being produced in this axis. Because these new supercells also do not have any implications for the  $c$  axis, it can be thought that these units will form “slabs” of supercells which stretch infinitely in  $b$  and  $c$ , while partially ordering in  $a$ . This “slab” nomenclature is taken from a study of strontium barium niobate, whose incommensurate structure is reported to be compiled of similarly ordered “slabs” of supercells.<sup>[22]</sup> These slab-like units can theoretically have any thickness in  $a$

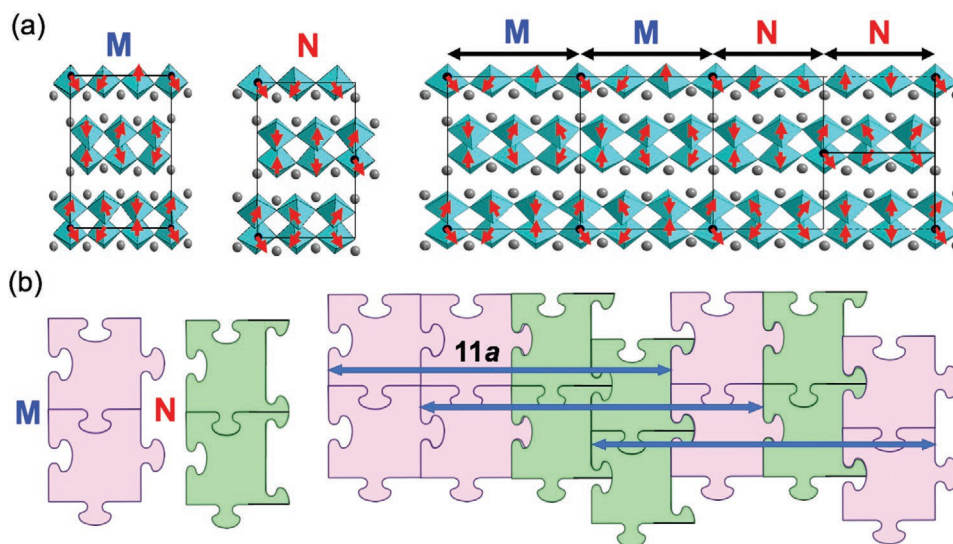


**Figure 6.** a) Suggested structural units built from diffraction data. The incommensuration originates from the partial ordering of the M and N supercells in the  $a$  axis. The M unit is a  $3 \times$  expansion of the basic cell in  $a$  and N unit is a  $2.5 \times$  expansion. Red arrows denote the rough tilting direction of the  $\text{TaO}_6$  octahedra and highlight equivalent octahedra that are created by translational symmetry. b) Illustration of the relationship between each block and adjacent layers; where M blocks will stack directly along  $a$  and N blocks will shift adjacent blocks by  $1/2$  unit cell in  $b$ . A combination of two of each block yields an  $11a$  supercell, a close approximate of the incommensurate wave vector observed by PND.

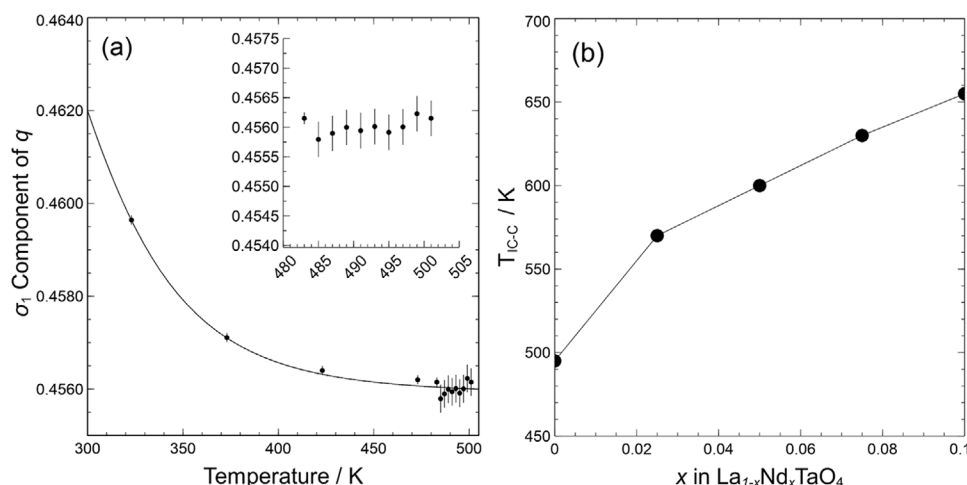


**Figure 7.** a) Incommensurate modulation vector,  $q$  along the  $a$  axis of the orthorhombic  $Cmc2_1$  phase as a function of temperature; zoom in of  $q$  close to the transition (inset). b) Temperature of IC-C transition ( $T_{IC-C}$ ) as a function of Nd doping showing increased stability of the IC phase with increasing Nd content.

but HRTEM images in the present work suggest they have very limited ordering and extension, due to generation and relaxation of the lattice strain.

As previously mentioned, comparisons can be drawn with  $La_2Ti_2O_7$ , which has an incommensurate layered perovskite structure which is made up of different structural units—similar to that suggested here for  $LaTaO_4$ . Despite the similarities,  $La_2Ti_2O_7$  has been shown to have a continuous displacement of La and accompanying tilt of octahedra, which over the course of the modulation wave results in a combination of the basic high-temperature and low-temperature unit cells stacking alongside each other in the  $a$  axis.<sup>[2]</sup> For  $LaTaO_4$  this would mean the LT phase would consist of units of orthorhombic (HT) and monoclinic ( $m$ - $LaTaO_4$ ) phases. There is no evidence of this from this study and hence this possibility has not been pursued further.

## 2.5. Temperature Dependence of $q$

From refinement of the neutron data it is observed that the modulation has a clear temperature dependence. Refinement of  $q$  at various temperatures shows the fractional coordinate of the modulation in  $a^*$ ,  $\sigma_1$ , decreases over the measured temperature range (Figure 7a). The approximate commensurate supercell at 483 K is  $11a$ , whereas at 323 K the approximate supercell is  $21a$ . This trend can be interpreted to suggest a greater degree of ordering as we increase in temperature and approach the transition into the commensurate HT phase. At temperatures close to the transition, shorter acquisition times and resulting poorer signal-to-noise ratio in the diffraction data, coupled with decreasing intensity of the satellite peaks, means accurate fitting of the satellite peaks is increasingly difficult but still give values consistent with this trend.

This shows the continuous relationship between the modulation and temperature, where decreasing temperature sees the value of  $q$  increase. It is noted that some previous studies of  $BaMnF_4$  have misinterpreted the relationship between temperature and  $q$ , where a “Devil’s staircase” was only revealed when

studying single crystals of higher quality than that of previous investigations.<sup>[10]</sup> Powder methods obviously lack the same accuracy as analysis of a single crystal and so the seemingly continuous relationship seen in Figure 7a should be taken as an approximation of the temperature dependence of  $q$ . A characteristic jump between lock-in values may not be evident in the current data and hence the possibility of a “Devil’s staircase” should be investigated further in future work.

## 2.6. Effects of Doping

Comparison of materials produced in this study with that of previous studies show a clear trend in the persistence of the modulation and the size of A cation. The monoclinic phase was stabilized by 10% Nd doping in an investigation by Cordrey et al.<sup>[5]</sup> and the accompanying dielectric data reveals that the IC to C transition does not occur until  $\approx 673$  K, around 170 K higher than in the undoped material. In order to investigate this more closely a number of Nd-doped compositions,  $La_{1-x}Nd_xTaO_4$  with  $x = 0.025, 0.05, 0.075,$  and  $0.1$  were prepared. In the absence of PND data for these samples the IC/C transition temperature ( $T_{IC-C}$ ) was simply monitored using dielectric spectroscopy. The data show a systematic increase in  $T_{IC-C}$  as function of  $x$ , Figure 7b, and illustrate the correlation between the degree substitution of smaller Nd cations at the A sites and stabilization of the modulation. This can be simply rationalized in terms of optimization of A site bonding environment as the structural driving force for the modulation; the smaller Nd cations will be even more underbonded than La and therefore displace to a greater degree. The larger displacement of these atoms required to optimize bonding stabilizes the modulated structure. It would be interesting however, to investigate the effect of Nd-doping on the magnitude of  $q$ .

## 3. Conclusion

Re-examination of  $LaTaO_4$  by electron microscopy and variable temperature powder neutron diffraction reveals that the



orthorhombic  $Cmc2_1$  structure is incommensurately modulated below 483 K. On heating, the material undergoes a transition to a commensurate  $Cmc2_1$  structure. This transition is the unidentified origin of the peak observed in dielectric data in previous studies. Electron and neutron diffraction data indicate the IC modulation is best described as  $q = (\approx 0.456, 0, 0)$  (at 483 K) resulting in the 4D superspace group  $Cmc2_1(\alpha 00)0s0$ . Although this approximate cell doubling in  $a$  is reminiscent of that observed in isostructural  $BaMnF_4$ ,<sup>[17]</sup> it is important to note the alternate space group settings: in  $BaMnF_4$  the modulation occurs along the polar axis, whereas in  $LaTaO_4$  the modulation (while still in the plane of the octahedral sheets) is orthogonal to the polar axis and hence closer comparisons can be drawn with the modulation of the  $n = 4$  oxides such as  $Sr_2Nb_2O_7$ . The origin of the modulation may be similar to that in  $Sr_2Nb_2O_7$ , whereby the A-cation (La) positions are modulated as a means to rectify the unusual bonding environment of the A sites in between octahedral layers. In contrast to  $Sr_2Nb_2O_7$ , however,  $LaTaO_4$  does not have the same continuous modulation of atomic positions incommensurate to the basic unit cell but instead the incommensuration arises from disordered stacking of larger structural units in  $a$ . A model for these units, M and N, have been proposed as  $3a$  and  $2.5a$  supercells, respectively, to demonstrate the principle of the formation of the incommensurate superstructure. Observation of a relationship between A-cation size and the IC transition has further alluded to irregular bonding within the structure and the structural units identified may be distorted from the basic  $Cmc2_1$  model in a way which is energetically beneficial and optimizes the La bonding environment. Observation of the modulation vector at varying temperature shows a reduction in the magnitude with increasing temperature, suggesting that the ordering of the M and N units improves as the IC-C transition is approached.

## 4. Experimental Section

**Synthesis:** All reagents (>99% purity) were dried for 1 h prior to use:  $La_2O_3$ ,  $Nd_2O_3$  at 1000 °C, and  $Ta_2O_5$  at 600 °C. Stoichiometric amounts of the oxides were mixed by milling at 600 rpm for 1 h in a planetary ball mill and pressed into 10–13 mm diameter pellets either under 1 tonne uniaxial load or 200 MPa of isostatic pressure. Pellets were then annealed at temperatures between 1350 and 1650 °C for 6 h.  $o$ - $LaTaO_4$  was favored by uniaxial pressing and annealing at 1350 °C, whereas the  $m$ - $LaTaO_4$  was most prevalent when annealing under the harsher conditions of isostatic pressing and annealing at 1650 °C. Both  $o$ - $LaTaO_4$  and  $m$ - $LaTaO_4$  were stabilized at room temperature purely by varying annealing conditions. Siqueira and Dias<sup>[9]</sup> had previously reported milder reaction conditions when producing the monoclinic polymorph of  $LaTaO_4$  but similar conditions have yielded mostly an orthorhombic phase in this study. Powder neutron diffraction (PND) data later showed that although this promotes crystallization into the orthorhombic form, a minor phase of the monoclinic structure is still produced ( $\approx 10\%$ ).

**Sample Characterization:** PND data were collected using the high-resolution powder diffractometer (HRPD) at ISIS. Data were collected on cooling from 523 K at 2 K increments to 483 K, for close observation of the IC-C phase transition—collection time for each time was 1 h (40  $\mu$ Ah integrated proton current to the target), except 483 and 523 K which was 3 h (120  $\mu$ Ah). Data were also collected between 473 and 323 K at 50 K increments for observation of the modulation of vector as a function of temperature—all collection times were 3 h (120  $\mu$ Ah). Collection on cooling was performed to eliminate monoclinic impurities

in the orthorhombic sample at lower temperatures.  $\approx 5$  g of sample was analyzed.

In-house PXRD was conducted using a PANalytical Empyrean Cu X-ray tube diffractometer with a primary beam monochromator (CuK $\alpha$ 1) and X'celerator RTMS detector. Both PXRD and PND data were refined by the Rietveld method using GSAS software.<sup>[23,24]</sup> Jana2006<sup>[25]</sup> was used in determining the modulated structure from variable temperature PND data. The modulation vector is typically presented as  $q = (\sigma_1, \sigma_2, \sigma_3)$ , where each sigma value represents a fractional coordinate with respect to reciprocal unit cell axes  $a^*$ ,  $b^*$ , and  $c^*$ , respectively.

SAED patterns and HRTEM images were recorded using a Gatan 794 CCD camera on a JEOL JEM-2011 electron microscope fitted with a LaB<sub>6</sub> filament operating at an accelerating voltage of 200 kV. For sampling, specimens were ground into powder in acetone with a pestle and mortar. A copper grid coated with a thin holey carbon film was used to support the powder sample.

## Acknowledgements

The authors thank the Science and Technology Facilities Council (STFC) for the provision of neutron diffraction facilities at ISIS (HRPD experiment RB1820307, <https://doi.org/10.5286/ISIS.E.RB1820307>) and the School of Chemistry, University of St Andrews for funding of a studentship to GWH through the EPSRC doctoral training grant (grant No. EP/K503162/1). SW thanks China Scholarship Council and University of St Andrews for a CSC-St Andrews Scholarship. This work was also facilitated by funding provided by the EPSRC (grant No. EP/P022637/1).

## Conflict of Interest

The authors declare no conflict of interest.

## Keywords

dielectrics, ferroics, structure–property relationships

Received: June 1, 2020

Revised: July 2, 2020

Published online:

- [1] P. Daniels, R. Tamazyán, C. A. Kuntscher, M. Dressel, F. Lichtenberg, S. van Smaalen, *Acta Crystallogr., Sect. B: Struct. Sci.* **2002**, 58, 970.
- [2] N. Ishizawa, K. Ninomiya, J. Wang, *Acta Crystallogr., Sect. B: Struct. Sci., Cryst. Eng. Mater.* **2019**, 75, 257.
- [3] M. Eibschütz, H. J. Guggenheim, S. H. Wemple, I. Camlibel, M. DiDomenico, *Phys. Lett. A* **1969**, 29, 409.
- [4] K. Shimamura, E. G. Villora, H. Zeng, M. Nakamura, S. Takekawa, K. Kitamura, *Appl. Phys. Lett.* **2006**, 89, 232911.
- [5] K. J. Cordrey, M. Stanczyk, C. A. L. Dixon, K. S. Knight, J. Gardner, F. D. Morrison, P. Lightfoot, *Dalton Trans.* **2015**, 44, 10673.
- [6] Y. G. Abreu, K. P. F. Siqueira, F. M. Matinaga, R. L. Moreira, A. Dias, *Ceram. Int.* **2017**, 43, 1543.
- [7] A. Yamamoto, T. Janssen, A. Janner, P. M. de Wolff, *Acta Crystallogr., Sect. A: Found. Crystallogr.* **1985**, 41, 528.
- [8] D. E. Cox, S. M. Shapiro, R. A. Cowley, M. Eibschütz, H. J. Guggenheim, *Phys. Rev. B* **1979**, 19, 5754.
- [9] J. F. Scott, R. Blinc, *J. Phys.: Condens. Matter* **2011**, 23, 1.
- [10] P. St-gregoire, M. Barthes, R. Almairac, J. Nouet, J. Y. Gesland, C. Filippini, U. Steigenberger, *Ferroelectrics* **1984**, 53, 307.
- [11] M. Hidaka, J. F. Scott, J. S. Storey, *Phys. B+C* **1984**, 123, 291.

- [12] J. F. Scott, F. Habbal, M. Hidaka, *Phys. Rev. B* **1982**, 25, 1805.
- [13] M. Hidaka, T. Nakayama, J. F. Scott, J. S. Storey, *Phys. B+C* **1985**, 133, 1.
- [14] X. Q. Liu, G. J. Li, X. M. Chen, *Solid State Commun.* **2016**, 247, 31.
- [15] F. Vullum, F. Nitsche, S. M. Selbach, T. Grande, *J. Solid State Chem.* **2008**, 181, 2580.
- [16] K. P. F. Siqueira, A. Dias, *Mater. Res.* **2014**, 17, 167.
- [17] R. J. Cava, R. S. Roth, *J. Solid State Chem.* **1981**, 36, 139.
- [18] W. Z. Zhou, A. Porch, I. B. M. van Damme, D. A. Jefferson, W. Y. Liang, P. P. Edwards, *J. Solid State Chem.* **1990**, 88, 193.
- [19] W. Z. Zhou, D. A. Jefferson, J. M. Thomas, *Proc. R. Soc. London, Ser. A* **1986**, 406, 173.
- [20] W. Z. Zhou, *J. Solid State Chem.* **2002**, 163, 479.
- [21] M. Hidaka, M. Yoshimura, H. Nishimori, H. Fujii, J. Y. Choi, Y. J. Park, J. H. Park, K. B. Lee, *Phase Transitions* **2001**, 73, 503.
- [22] L. A. Bursill, P. J. Lin, *Acta Crystallogr., Sect. B: Struct. Sci.* **1987**, 43, 49.
- [23] R. B. Von Dreele, A. C. Larson, *General Structure Analysis System (GSAS)*, Los Alamos National Laboratory, xxx **1994**, LAUR 86-768.
- [24] B. H. Toby, *J. Appl. Crystallogr.* **2001**, 34, 210.
- [25] V. Petříček, M. Dušek, L. Palatinus, *Kristallogr. – Cryst. Mater.* **2014**, 229, 345.